LA-UR-14-28872 (Accepted Manuscript)

The Shock/Shear platform for planar radiation-hydrodynamics experiments on the National Ignition Facility

Doss, Forrest William; Kline, John L.; Flippo, Kirk Adler; Perry, Theodore Sonne; DeVolder, Barbara Gloria; Tregillis, Ian Lee; Loomis, Eric Nicholas; Merritt, Elizabeth Catherine; Murphy, Thomas Joseph; Sherrill, Leslie Welser; Fincke, James R.

To be published in: Physics of Plasmas, Vol.22, iss.5, p.056303, May 2015.

DOI to publisher's version: 10.1063/1.4918354

Permalink to record: http://permalink.lanl.gov/object/view?what=info:lanl-repo/lareport/LA-UR-14-28872

LA-UR-14-28872, *Physics of Plasmas*, **22**, 056303 (2015)

The Shock/Shear platform for planar radiation-hydrodynamics experiments on the National Ignition Facility

F. W. Doss,[a] J. L. Kline, K. A. Flippo, T. S. Perry, B. G. DeVolder, I. Tregillis, E. N. Loomis, E. C. Merritt, T. J. Murphy, L. Welser-Sherrill, and J. R. Fincke
Los Alamos National Laboratory, New Mexico, 87545, United States

An indirectly-driven shock tube experiment fielded on the National Ignition Facility (NIF) was used to create a high-energy-density hydrodynamics platform at unprecedented scale. Scaling up a shear-induced mixing experiment previously fielded at OMEGA, the NIF shear platform drives 130 μm/ns shocks into a CH foam-filled shock tube ($\sim$60 mg/cc) with interior dimensions of 1.5 mm diameter and 5 mm length. The pulse-shaping capabilities of the NIF are used to extend the drive for $>$ 10 ns, and the large interior tube volumes are used to isolate physics-altering edge effects from the region of interest. The scaling of the experiment to the NIF allows for considerable improvement in maximum driving time of hydrodynamics, in fidelity of physics under examination, and in diagnostic clarity. Details of the experimental platform and post-shot simulations used in the analysis of the platform-qualifying data are presented. Hydrodynamic scaling is used to compare shear data from OMEGA with that from NIF, suggesting a possible change in the dimensionality of the instability at late times from one platform to the other.

I. INTRODUCTION

Shock tubes have been used to investigate hydrodynamic instabilities such as Rayleigh-Taylor[1,2], Richtmyer-Meshkov[3,4], and Kelvin-Helmholtz[5,6] with liquids and gases in numerous experiments since the 1950s. Such work continues today with more advanced diagnostics and experimental configurations that enable observation of the growth of these instabilities and their ability to induce mixing of initially separated materials. While these experiments provide excellent tests of theoretical models for turbulent mixing in the aerodynamic regime, these experiments do not include physical processes, such as ionization and plasma kinetics or strong radiation transport, which can occur and at times dominate in more extreme systems such as astrophysical events or inertial confinement fusion implosions, nor do they have access to the extremely high variation in material properties, especially density, that can be found in these applications. Over the last twenty years, shock tube experiments have been adapted[7–11] to study fluid instabilities under High-Energy-Density Physics (HEDP) conditions (i.e., physics above 1 Mbar[12]) driven by the kJ-class laser systems such as the Nova[13] and OMEGA[14] lasers. Experiments in the HEDP regime are typically plasmas and have the advantages of machining and assembling initially solid targets for additional control over initial conditions at interfaces and allowing access to a larger range of density ratios. Challenges to such experiments stem from the limits on energy available to drive the target into the HEDP regime; limited volumes which may be driven to the requisite energy density lead to the influence of walls on the experiment, and limited duration of the drive leads to the experiment being driven by unsupported shocks with decaying strength. The National Ignition Facility[15] (NIF), with its MJ-class drive capability, can reduce the influence of these deleterious effects and open a much wider range of parameter space in which to study fluid instabilities under HEDP conditions.

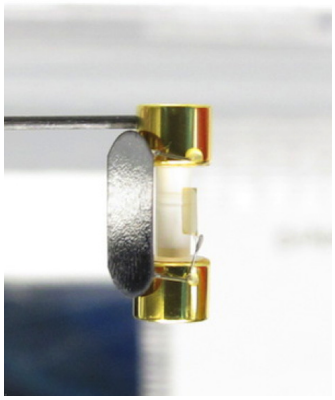

FIG. 1. A LANL Shock/Shear target for NIF.

Los Alamos National Laboratory's HEDP Shock/Shear platform was originally developed as a directly-laser-driven shock tube platform with interchangeable geometries to be fired at the OMEGA Laser Facility. The target exterior, diagnostic scheme, and drive pulse shape and energy were all fixed while the tube interiors were changed to various geometries which could explore various physics issues[16], various scenarios of Richtmyer-Meshkov and Kelvin-Helmholtz instability growth most frequently. This platform was then used in a counterpropagating shear experiment[17,18] in which two shocks cross in the tube center on either side of an aluminum tracer strip. The expansion of the strip under the resulting shear instability was then measured. The $\sim$1.4 mm long and 0.5 mm ID beryllium shock tubes were fitted with ablators to launch 110 μm/ns shocks with $\sim$4 Mbar post-shock pressures and 70 μm/ns

[a] Electronic mail: fdoss@lanl.gov

post-shock flow speeds from each side of the tube. By fielding identical exterior components across campaigns, and by delivering the same 4 kJ, 1 ns laser profiles to each end of the tube, the targets were kept extremely similar from the point of view of the laser facility, which accelerated both design and experimental review time. This platform was used, with variations such as including streak radiography or swapping the aluminum strip for a disc in Richtmyer-Meshkov configuration, to explore issues including thermodynamics-turbulence coupling[18], growth of a Kelvin-Helmholtz shear layer from a shock-compressed minimum[19], and as a source of validation data for development of new techniques in large-eddy-simulations[20,21].

The new NIF platform (pictured in Figure 1) represents an effort to scale the successes of the Shock/Shear platform from OMEGA to cleaner experiments and new regimes permitted by the superior drive capabilities of the NIF[22]. The platform development shots described in this paper produce shocks with speed 130 μm/ns, 10 Mbar post-shock pressures, and 110 μm/ns post-shock flow speeds, placing the experiments in a similar regime as the preceding OMEGA experiments, to develop the platform and extend our existing data before introducing any significant new physics effects. The quantitative applications of this scaling is addressed in greater detail in Section V. The shock tubes, now 5.2 mm long and 1.5 mm ID, are filled with the same 60 mg/cc foam as used in many of the OMEGA experiments. In a modification from the OMEGA experiments, the tube is fitted with gold hohlraums with a single laser-entrance hole (halfraums) on either end, which use the cylindrically symmetric beam arrangement at the NIF in a natural manner – the target is aligned vertically in the chamber, contained within the safe zone void of unconverted light. The halfraums are now used to drive the target for 10 ns, allowing for longer survival of the hydrodynamics and cleaner implementations of the desired physics by delaying the rarefactions and pressure drops from an impulsive drive. A unique backlighting solution was implemented to take advantage of the new geometry and substantially greater energy available on the NIF, and also to overcome the tube material's changing from beryllium to plastic.

The initial platform shots reported here delivered 300 kJ into each halfraum. By shortening the 10 ns pulse and increasing the drive power, considerably stronger shocks could be launched. The platform has been designed to be extended to these more intense regimes in the future, and to potentially be host to a variety of internal configurations studying diverse physics interests.

II. EXPERIMENT DESIGN

Schematically depicted in Figure 2, the target consists of a cylindrical plastic shock tube linking two hohlraum volumes. These halfraums are designed to receive approximately 300 kJ of laser energy over the course of

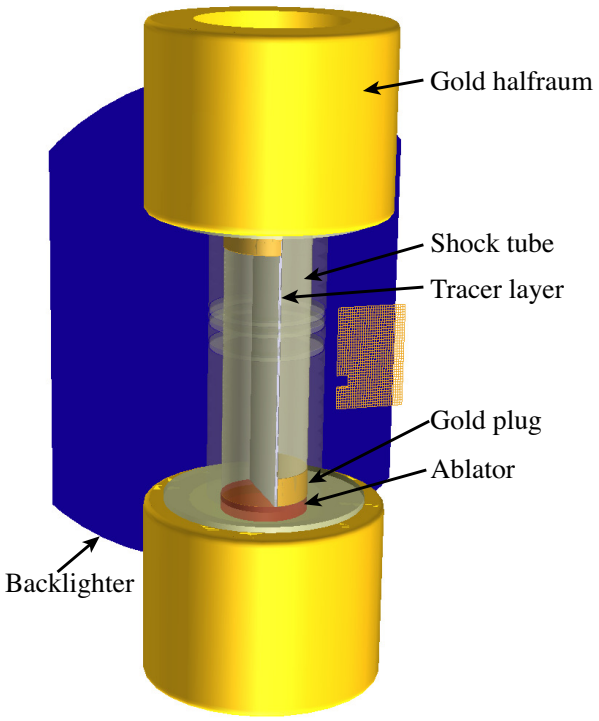

FIG. 2. A VISRAD[23] rendering of the target, displaying (gray) the shock tube with enclosed metal plate with (yellow) gold plugs embedded on either end and a gold fidcuial grid off to the right side. The gold hohlraums on the top and the bottom provide indirect shock drive to the tube by driving the (brown) plastic ablator layer, and the backlighter (blue) is used to diagnose the experiment.

11 ns, sustaining a radiation temperature of up to 250 eV in order to drive the hydrodynamics in the tube. The shock tube contains two hemi-cylinders of light CH foam (60 mg/cc), an aluminum strip (initial width 40 μm), and one gold plug on each side placed at opposite ends of the tube which serve as collimators for the shocks. The principal outcome of the experiment is to diagnose the evolution of the aluminum strip as it becomes shocked and evolves under the subsequent shear instability.

Each side also is capped with a polystyrene ablator (1.4 g/cc) 270 μm thick. The ablator thickness has been chosen to ensure that for the entire duration of the hohlraum drive enough unablated mass remains to both act as a continuous piston on the light foam and to retain the bulk of the radiation drive from streaming through the system. The ablator is doped uniformly with 1.0$\pm$0.1% silicon to prevent high-energy components of the hohlraum emission from streaming into the tube early in time. The shock tube is 5.2 mm long, 1.5 mm ID, and has a wall thickness of 0.25 mm. The wall thickness was constrained by the need to confine the tube center against radial disassembly until at least 30 ns, and otherwise minimized to avoid unnecessary loss of backlighting signal.

The laser pulse used to drive the hohlraums is designed

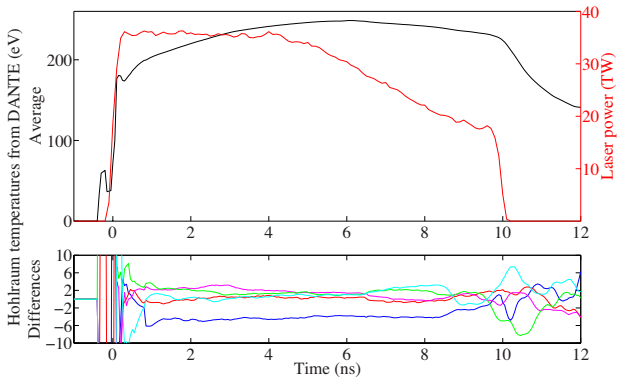

FIG. 3. (above) Average of five drive pulses into the top halfraums listed in Table I as reported by Dante along with (red) the laser power driving the hohlraum, and (below) the difference of each temperature record from the average.

to drive approximately steady post-shock conditions for as long as possible. The drive lasts for 10 ns. For the first 4 ns, the laser drive is constant, and the hohlraum radiation temperature is increased to 250 eV. When it reaches that peak, the laser drive is relaxed into a reverse ramp and gradually declines, keeping the hohlraum temperature approximately steady. Peak driving conditions are timed to coincide with the breakout of the shock from the ablator, after which the shock is driven steadily. Figure 3 shows the average and differences of Dante[24,25] records for five platform development campaign shots and the laser pulse for an actual shot. Shot-to-shot variation during the main drive segment from 2 ns to 10 ns are within ±2 eV. Shots not including Shot N131115, from which one entire bundle of drive beams was dropped (effectively the worst-case scenario while still allowing the shot to go forward), have characteristic variation of ±0.4 eV. The data shown in Figure 3 are shifted by as much as 200 ps to align the maxima of each radiation temperature with the average for direct comparison. For comparison, the time resolution of the Dante instrument is 150 ps[26].

Table I shows the actual energies recorded going to each halfraum for three shots. Inconsistencies in operating conditions from day to day yield small variations in energy from shot to shot, in addition to similar variations from top to bottom within a single shot. Our rules of engagement specified matching the requested energy to within 5% on each side, to keep overall symmetry within 10%. Drive symmetry as delivered was typically within 2% and was 5% at worst (the effects of which are described later). Based on the radiography obtained, backlighter signal was preferred at the design energy 130 kJ and noticeably degraded but still clear at 110 kJ.

The attached Big Area Backlighter (BABL) was designed for this experiment[27] and uses 130 kJ of laser energy to produce a large uniform area (∼2.5 mm by 3 mm) of x-ray emission. Iron was used to emit at the 6.7 keV He-α-like line for radiography with the intention

TABLE I. Energy delivered to each target site (kJ) and centered strip timing (ns) by shot. The energies delivered to the top and bottom halfraums and backlighter (BL) are each enumerated separately.

	N131115	N140506	N140117	N140507	N131206
Top (kJ)	289	304	313	302	311
Bottom	288	307	298	304	305
BL	131	132	117	134	112
Time (ns)	17.0	20.1	22.4	25.0	27.8

of obtaining good contrast through the thick plastic tube walls. The data is then recorded on two independently timed micro-channel-plate strips, arranged so that the long direction of the strip is aligned with the long axis of the shock tube. Figures 4 and 7 show data recorded by radiography from several shots. Each shot also obtains two strips of gated framing camera data separated by 1.2 ns.

III. ANALYSIS OF RADIOGRAPHY

In this section we examine the radiographic data from a particular shot in greater detail to demonstrate our method. Figure 4 displays typical radiography from one shot together with annotations describing the process of extracting data from the image. The white box indicates notches, 100 microns wide and 50 microns deep, machined in the shock tube. The second half of the figure shows the lineout down the box, averaged in the lateral direction. Fitting the shape of the transmission to the geometry machined into the tube generates values for the absolute spatial location of features as well as calibration of spatial scales. The inter-notch spacing, with its characteristic dot-dot-dash-dot spacing, provides particularly good constraints on pixel-to-micron scaling factors, which agree with and validate other methods of determining this value (including absolute magnification estimates of the instrument and diagnostic scheme, and periodic spacing in the gold grid). The locative data contained in the notches is guaranteed to exist in the plane of the data, to be free of early time preheat effects which may influence the gold grid, and is preferred whenever possible, typically until late time hydrodynamics affects the notches. In Figure 4, looking across the tube from left to right, one can see the notches, unaffected on the left side of the tube, inverting and becoming jets on the right side as the shock breaks out of the tube.

Shock location is measured by following the transmitted component of the shocks in the wall until they meet the tube interior. This data is used below in Section IV to estimate our fidelity of simulation of the drive conditions for the platform. For the bulk of the duration of the experiment, post-shock simulations suggest that the shocks are close to planar in each hemi-cylindrical volume and that this is a good method for assigning shock

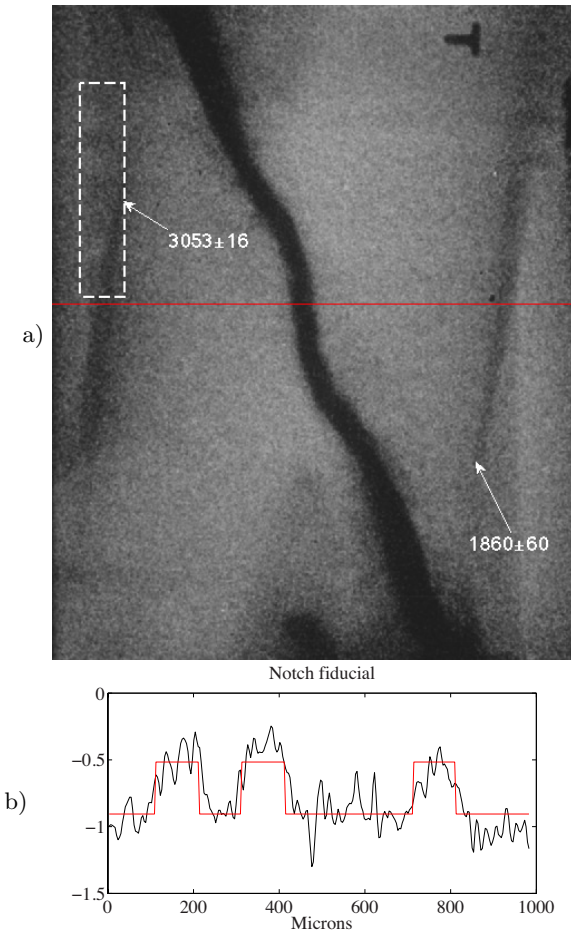

FIG. 4. a) Data from the N140117 radiograph. The white dashed box indicates the region used for spatial calibration by notch recognition. The red line indicates the shock tube centerline, as determined by the spatial calibration. Arrows indicate absolute locations (in μm) of the termination of shock components in the wall. The "T" at the top is a diagnostic orientation fiducial.
b) Lineout of transmission (arbitrary units) down the notch-containing box (black) together with the expected signal from the notches machined into the shock tube (red).

location. Error in the measurement is estimated from goodness-of-fit of sharply decreasing profiles to actual lineouts along the shocks in the walls. When noise and contrast are good, this typically produces uncertainty of around 20 μm, comparable to the resolution measured in our backlighter test[27]. When contrast is lowered, the uncertainty rises due to the increasing ambiguity of the fit to the transition in signal. When multiple redundant pinhole images are used, the error can sometimes be improved by combining independent images of the same shock. From the fit of the notch pattern to the lineout, the uncertainty in absolute location is negligible, on order 1 μm in shots with a clear notch sequence in the data.

IV. MODELING

The postshot and design radiation hydrodynamics simulations were performed in the LANL Eulerian code RAGE[28]. Figure 5 shows simulated output from a representative post-shot simulation.

In order to provide an engineering match to data and create a description of the drive suitable for modeling subsequent experiments on this platform, two multipliers were applied to the flux delivered from the halfraum to the shock tube, one for the overall drive, and one for the high-energy components of the drive. These were estimated by the shock locations as a function of time and by the measurement of preheat, discussed below.

A. Preheat

In order to quantify the effect of preheating from high-energy x-ray emissions from the hohlraum upstream, a notoriously difficult situation to model from first principles due to its strong connection to laser-plasma interactions at the hohlraum wall, the pre-hydrodynamic behavior of the layer was measured in Shot N131115. This radiograph was taken before the shocks have reached the tube center, and the expansion of the layer up to that point was driven by the upstream heating from the drive. The layer temperature was then inferred from postshot simulations that matched the layer width at that time.

Experimentally, to reduce the effect of the high-energy components of the gold emission, silicon dopant was added to the polystyrene ablator caps at either end. Since the effects of this change in composition would be later subsumed by the empirical scaling factor, no effort was made to model it directly. The effective preheat in the experiment was then estimated as a fraction of the simulated preheat in the case where no silicon absorbent was present, and represented in the simulation as a multiplier on the x-ray flux into the tube for photon energies above 2.5 keV. The extra heating allowed by the deposition of that energy into the ablator by the dopant would similarly be absorbed into the multiplier for overall flux.

Comparisons to data found that the experimental case with the absorbent performed as if it had 20% of the high-energy flux as the simulated case without absorbent. This lowered the heating of the layer to 0.5 eV from a simulated 2 eV with no dopant. Because of this the layer, which does not expand early in time as rapidly at this lower temperature, remains at considerably thinner widths than were projected in early designs[22]. This degree of preheat was found to be comparable to that inferred in the OMEGA experiment.

B. Drive

The positional data from the shots discussed above (specifically the N140117 intermediate time data) was

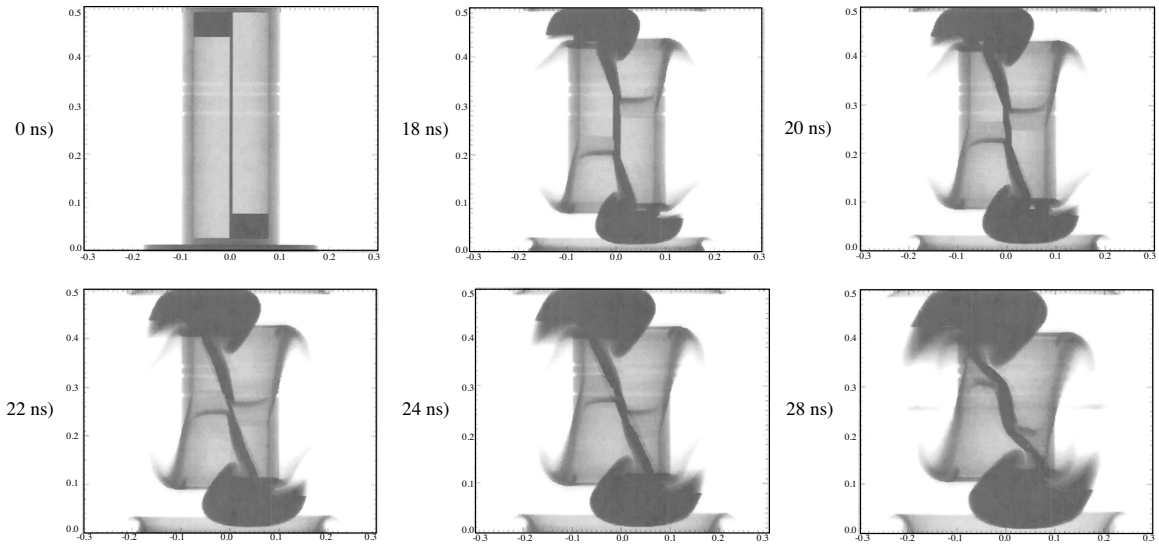

FIG. 5. Synthetic radiographs from RAGE simulations of the NIF counterpropagating shear experiment. Coordinates in cm. The aluminum strip is the dark feature running from top to bottom which spreads at late times. Both the shocks which travel from the top and bottom as well as the dark arc of ablator material trailing behind the shocks are visible in the synthetic radiographs. In the experiments neither of these features are typically visible and the shock is located by finding the points of termination of the transmitted shocks in the wall.

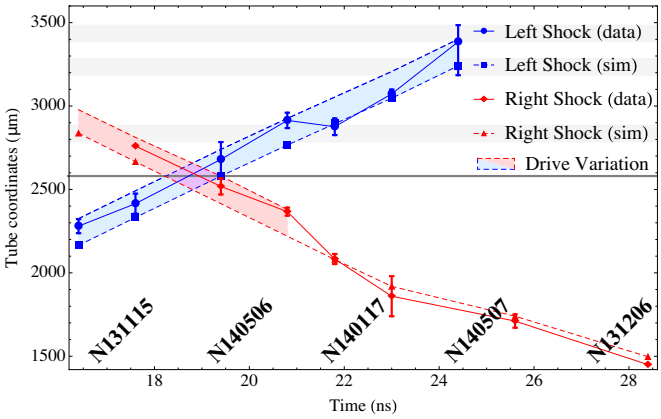

FIG. 6. Positional data from shots and simulations. Error bars shown between 16 to 24 ns are derived from sharpness in detecting the termination of the shock in the wall. The shaded region shows variation in simulated shock position from the nominal to observed drive. The right shock simulation shown with red triangles was calibrated to the drive asymmetry in N140117 (see Table I). The gray line represents the tube center, and the light gray regions in the top half correspond to the location of the notch features machined into the tube.

used to calibrate post-shot the drive via a flux multiplier at the few-percent level. In order to accommodate the reported difference in drive energy (15 kJ), the top and bottom hohlraum multipliers were allowed to be different. Starting from a simulation calculated with the nominal laser drive of 300 kJ, outgoing flux multipliers of 0.97 on the bottom and 1.09 on the top were used in the simulation used in Figure 6. That these effective flux multipliers were found to be higher than the actual difference in delivered energy (5%) may be an effect of possible nonlinearities in laser-to-ablator coupling efficiency with these hohlraum temperatures and pulse shapes due to e.g. losses to heating the hohlraum wall[29].

The predicted shock positions in both directions are compared with data in Figure 6 (the data placed at 28.4 ns is not actually the shock position at that time, but a record of where the shock interacted with the wall and the refracted component of the opposing shock. The shock itself is too non-planar at this time to be assigned a simple scalar location). These drive parameters will be used to design future experiments and predict features, such as the shock crossing time and minimum layer time, for future versions of this experiment. Based on the simulations at different drive energies, the shocks are simulated to have traveled with speed between 110 and 130 μm/ns, and the data is consistent with a mean shock speed of 120 μm/ns.

The drive energy asymmetry in N140117 (as recorded in Table I) is taken to be typical of the possible shot-to-shot drive variation. Running separate simulations in which the drive asymmetry is reversed, the mean difference in shock locations due to this variation in driving power is $\sim$160 μm. These variations in drive are shown in Figure 6 as shaded regions. To the extent that drive variation for future shots stays within the envelope established in N140117, these shaded regions represent the preshot uncertainty in shock location. These simulations were used to predict the locations of shocks in N140506 and N140507, which fell within the expected limits for lower drive on the right shock and higher drive on the left shock compared to N140117.

Based on the envelope of reasonable drive variation

thus defined, the experiment can be expected to fall within 80 μm of the center defined by the target geometry, i.e. that overdriving one halfraum with respect to the other effectively shifts the hydrodynamics by a maximum of 80 μm away from the geometric tube center. Similarly, simulations in which the left and right shocks have the same energy do not translate the hydrodynamics in space but instead shift the shock crossing time to a value between 18.25 and 19.5 ns as a result of these drive variations, a predictive uncertainty of around a nanosecond in that feature.

V. LAYER WIDTH DATA

The primary metric of shear instability and mixing in these experiments is the layer width at tube center as a function of time. A sequence of radiographs are collected as described above, some of which are shown in Figure 7. The notches and grid are used to locate the tube center axially, and a lineout is taken along the radial direction. The lineout is averaged ten pixels in the vertical direction to improve signal, and fit to a gaussian line shape from which the two-sigma value is reported as halfwidth from the layer center to the extent of aluminum mixing. This is chosen to remain compatible with the 95% area-under-the-curve measurements taken in previous OMEGA campaigns[17] where distinct non-gaussianity of the lineout shapes required a more general method. The differences in pinhole resolution, imaging contrast from layer to foam, radiographic noise, and limb effects due to the tube between the two experiments favor the gaussian fit method at NIF.

A. Hydrodynamic Scaling

For the platform development campaign on NIF, the hydrodynamic responses were scaled such that the initial phases of the instability would behave equivalently between the two systems.

Before the onset of instability, the hydrodynamics is governed by the response of the metal layer to the shock passing over it. In order to ensure a similar response of the layer to conditions observed on OMEGA, the mass of the layer was increased along with the post-shock pressure. We can quantify the similarity using the concept of Euler scaling[30,31], in which hydrodynamic equivalence holds between systems in which the Euler number

$$\mathrm{Eu} = v\sqrt{\frac{\rho}{P}} = \frac{L}{\tau}\sqrt{\frac{\rho}{P}} \tag{1}$$

is equal, where v, L, τ, ρ, and P are respectively characteristic velocity, length, time, density, and pressure scales. Since the post-shock pressure was increased at NIF to $\sim$10 Mbar ($P_{\mathrm{NIF}} = 2P_\Omega$), and the length scale of the aluminum layer was increased from 20 μm to 40 μm ($L_{\mathrm{NIF}} = 2L_\Omega$) while the density was unchanged ($\rho_{\mathrm{NIF}} = \rho_\Omega$), scaling exists ($\mathrm{Eu}_{\mathrm{NIF}} = \mathrm{Eu}_\Omega$) when we consider time scales $\tau_{\mathrm{NIF}} = \sqrt{2}\tau_\Omega \approx 1.4\tau_\Omega$. That is, the initial response of the layer to the passing shock should be equivalent but proceed slightly slower on NIF due to the increased mass.

A similar scaling can also be quickly derived for the initial phases of the instability, when only the kinematic variables play a role and mass and pressure terms do not yet play a part in the evolution. During the linear phase of the instability, analytic derivation of the growth rate for this counter flowing geometry[17] yields

$$n = \frac{\sqrt{2}V}{efL} \tag{2}$$

where $e = 2.718\ldots$ and n, V, f, and L are the growth rate, flow velocity parallel to the layer, the fraction of the layer initially undergoing shear, and the initial layer thickness. For this shear instability, we can again construct from the dimensional quantities a similarity variable, KH, defined by suppressing non-dimensional factors as

$$\mathrm{KH} = \tau n = \tau\frac{V}{L}. \tag{3}$$

As above, the length scales at NIF are double those at OMEGA ($L_{\mathrm{NIF}} = 2L_\Omega$). As we reported in the Introduction, the post-shock flow speeds are increased at NIF from 70 μm/ns on each side to 110 μm/ns ($V_{\mathrm{NIF}} = 11/7 \cdot V_\Omega$). So once again, we achieve similarity during the initial shear phase ($\mathrm{KH}_{\mathrm{NIF}} = \mathrm{KH}_\Omega$) if we scale our time scales τ by $\tau_{\mathrm{NIF}} = 1.3\tau_\Omega$. This is close to and consistent with the timescale we obtained from Equation 1, which implies the equivalence in our two cases of the non-dimensional variable f we dropped, which relates to the internal structure of the compressed layer as set up by the shock evolution controlled by the Euler scaling above.

The NIF experiment is of course not hydrodynamically scaled to the OMEGA campaigns for its full duration, but only while the pressure profiles $P(t)$ imposed by the drive are the same (after applying the scaling) in both cases. The OMEGA experiments end either when the shocks are reflected off of the gold plugs and return to the center, or when rarefactions launched by the short life-time of the drive reach the tube center. The NIF experiment moves the boundaries of the experiment further away from the shear volume and sustains the drive ten times as long. In this way the NIF experiment, while displaying similar, scaled evolution at early times, extends into late times by eliminating the reflections and transients that limit the OMEGA configuration. The length and time scalings above ($L_{\mathrm{NIF}} = 2L_\Omega$, $\tau_{\mathrm{NIF}} = 1.3\tau_\Omega$) will be used below to directly compare the data between OMEGA and NIF campaigns in the applicable region.

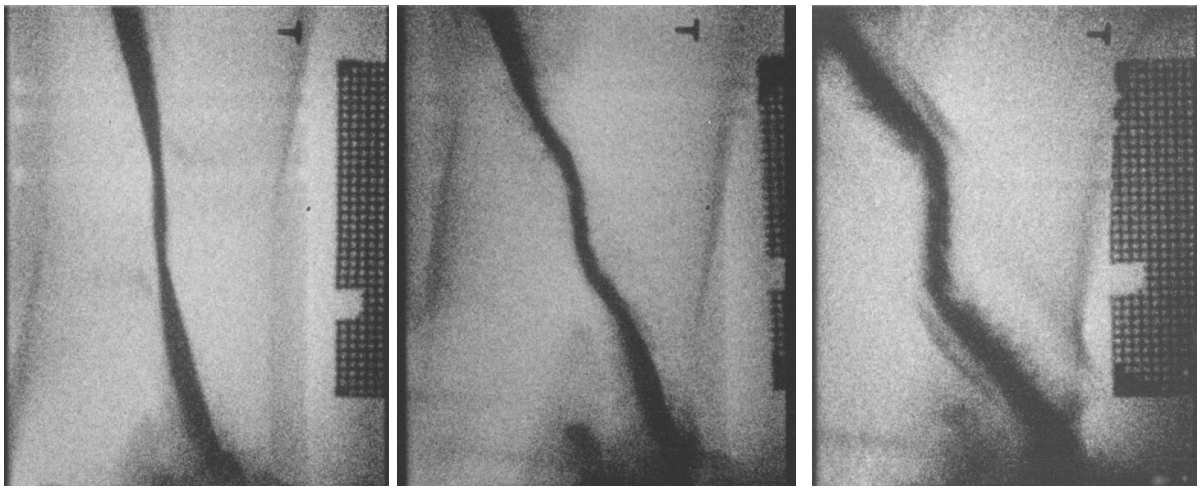

FIG. 7. Data from a single strip from each of shots (left to right) N131115 at 17.6 ns, N140117 at 23.0 ns, and N131206 at 28.4 ns. The dark aluminum tracer layer (running top to bottom) is seen to expand as time goes on under the influence of the shear instability, and to become more corrugated. At late times (far right) the non-central portions of the layer are seen to develop structure under a more complicated loading of shear and oblique shocks. On the opposite side of the layer, the transmitted shock from left-to-right through the oblique portion of the tracer layer is visible as a dark arc.

FIG. 8. Radiography from the 33.2-34.5 ns Shot N141006. Image quality was lowered due to the extra-thick tube used to achieve late time.

B. Late time data

In order to extend our dataset to late time (later than 30 ns), an additional target was recently fired (Shot N141006) in which several modifications were made to take data as late as 34.5 ns. In order to radially confine the tube wall longer than the 30 ns for which it was originally designed, the plastic wall thickness was increased from 250 μm to 500 μm. Also, in order to mitigate issues regarding optics damage for beamlines at the NIF, the laser pulse was modified to a different drive which produced essentially the same radiation temperature drive history in the halfraum. These changes are not believed to have altered the hydrodynamics of the experiment, though radiograph quality was sacrificed in part by moving to the thicker tube wall.

The data shown in Figure 8 shows the layer at very late times. Of particular interest in the data is the periodic structure which is observed to be forming in the layer, the possible implications of which will be discussed below. The emergence of a preferred single most-unstable mode from the length scale set by the initial layer thickness was predicted for these systems by analysis in Doss et al.[17] but not previously observed in edge-on radiography of the layer.

C. Scaled Data

Figure 9 shows the extracted width data from these NIF experiments and the two OMEGA campaigns for which scaling exists to these conditions[17,18]. Also shown is a best-fit RAGE simulation to the behavior of the OMEGA experiments. The left and bottom axes record length and time data, respectively, from OMEGA experiments, while the right and top axes show widths and times for NIF data. The scaling between these axes are such that the scaling of length and time scales in Equations 1 and 3 are observed. When this is done, the NIF and OMEGA datasets are seen to lie in good agreement from the initial shock crossing through the initial growth of the instability.

However, at late times, the NIF experiment appears to diverge from the predictions of the continued OMEGA experiments. A plausible reason for this, supported by the periodic mode structure appearing and persisting in Shot N141006 (Figure 8), is that the NIF experiment is remaining two-dimensional out to late times. The time at which the two campaigns diverge is around when the

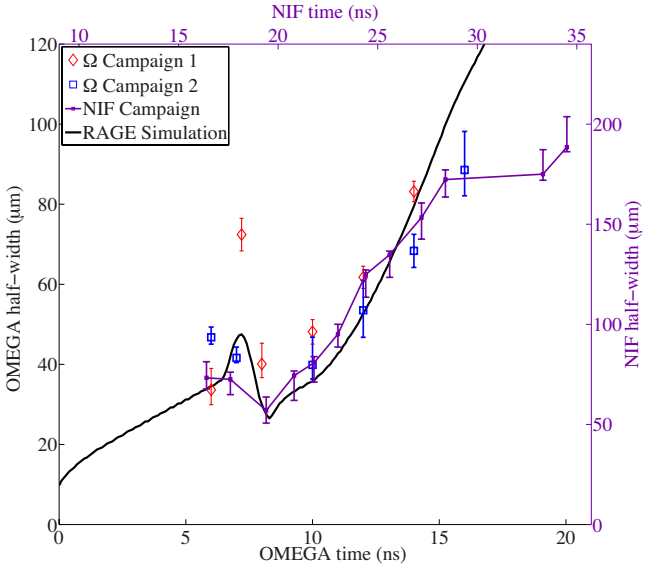

FIG. 9. Layer widths as a function of time at OMEGA and NIF. Left and bottom axes refer to widths and times of data from OMEGA, right and top axes show widths and times taken at NIF. The scaling between the two axes is such that the hydrodynamics are equivalent, as set by Equations 1 and 3 and the discussion in Section V A.

OMEGA campaigns, by analysis of a radiographic view orthogonal to the edge-on measurements shown here, were earlier reported to be developing three-dimensional structure[17]. This occurred in OMEGA at 14 ns, corresponding to ∼27 ns scaled time at NIF. Data after that point at OMEGA also show no persistence of periodic mode structure to late times as seen here. It is conjectured that the improved drive stability of NIF and ability to stage destabilizing edge-effects much further from the test sections as compared to OMEGA are allowing the instability to remain two-dimensional, a state which is known to reduce mixing-layer growth in shear systems beneath that of fully three-dimensional flow[32]. Future work including additional analysis of the layer widths, orthogonal views at both facilities, and dedicated experiments are planned to illuminate or confirm the situation.

VI. CONCLUSIONS

The LANL Shock/Shear platform has been developed to enable planar radiation-hydrodynamics experiments in shock tubes at the NIF. The platform leverages the facility's indirect drive technology by using double-ended halfraum drive to launch the hydrodynamics, and has been used for an experiment designed to take advantage of the long sustained drive capabilities the NIF drive offers. Good repeatability in drive conditions was demonstrated, with variation in energy between shots and ends of the targets staying within the 5% level, which suffices to maintain consistency in the resulting hydrodynamics. Diagnosing the experiments with the BABL was a success, using the iron emission lines from over 3 mm of area backlighting source to image the tube interior. Multi-strip detectors were used to obtain multiple images per shot, increasing the rate of data gathering. The radiographs obtained were of good quality and we were able to extract positional data of features which provided constraints to the drive modeling.

Hydrodynamic scaling can be used to connect the experiments from both OMEGA and NIF as long as they remain in the same physics regime and are undisturbed by influences not included in the scaling. Similar hydrodynamic evolution to that observed at OMEGA was shown to hold in the scaled sense at NIF from the initial crossing of the shocks at the tube center until a point in time at which the OMEGA experiments are observed to begin evolving three-dimensionally. Further investigation will be conducted into the differences in the experiments at late time and the nature of the edge-effects or transients which are presumably destabilizing the experiment in the smaller OMEGA target but absent in the NIF experiment, and should be expected to yield interesting results on the necessary conditions for vigorous multi-material mixing to occur in high-energy-density systems.

The platform was designed and analyzed in the Eulerian radiation-hydrodynamics code RAGE, which has allowed the drive and preheat to be calibrated empirically to a profile now allowing for the design of future experiments on the platform. The code results will be used in the future for the continued, detailed analysis of the shear-induced mixing dynamics of the present experiment.

ACKNOWLEDGMENTS

We would like to thank Dan Kalantar for useful fielding discussions, L Robin Benedetti for discussion on the x-ray framing cameras, Warren Hsing for useful discussion on planning the experiments for NIF, the NIF operations team, and Los Alamos target fabrication. The referee for this paper is also thanked for their comments and discussion. This work was supported by the U.S. Department of Energy and performed by Los Alamos National Laboratory, operated by Los Alamos National Security under Contract DE-AC52-06NA25396. NIF facility and experimental data reflects facility development and operations performed under the auspices of the U.S. Department of Energy by Lawrence Livermore National Laboratory under Contract DE-AC52-07NA27344

[1] Lord Rayleigh. Investigation of the character of the equilibrium of an incompressible heavy fluid of variable density. *Proceedings of the London Mathematical Society*, 14:170, 1883.

[2] Geoffry Ingram Taylor. The instability of liquid surfaces when accelerated in a direction perpendicular to their planes. *Proceedings of the Royal Society of London A*, 201(1065):192, 1950.

[3]R D Richtmyer. Taylor instability in a shock acceleration of compressible fluids. *Communications on Pure and Applied Mathematics*, 13:297, 1960.

[4]E E Meshkov. Instability of the interface of two gases accelerated by a shock wave. *Soviet Fluid Dynamics*, 4:101, 1969.

[5]Lord Kelvin. Hydrokinetic solutions and observations. *Philosophical Magazine*, 42:362, 1871.

[6]Hermann von Helmholtz. On discontinuous movements of fluids. *Philosophical Magazine Series 4*, 36(244):XLIII. 337–346, 1868.

[7]S. G. Glendinning, S. V. Weber, P. Bell, L. B. DaSilva, S. N. Dixit, M. A. Henesian, D. R. Kania, J. D. Kilkenny, H. T. Powell, R. J. Wallace, P. J. Wegner, J. P. Knauer, and C. P. Verdon. Laser-driven planar Rayleigh-Taylor instability experiments. *Physical Review Letters*, 69(8):1201, 1992.

[8]K. S. Budil, B. A. Remington, T. A. Peyser, K. O. Mikaelian, P. L. Miller, N. C. Woolsey, W. M. Wood-Vasey, and A. M. Rubenchik. Experimental comparison of classical versus ablative rayleigh-taylor instability. *Phys. Rev. Lett.*, 76:4536, 1996.

[9]O A Hurricane, J F Hansen, H F Robey, B A Remington, M J Bono, E C Harding, R P Drake, and C C Kuranz. A high energy density shock driven Kelvin-Helmholtz shear layer experiment. *Physics of Plasmas*, 16:056305, 2009.

[10]E C Harding, J F Hansen, O A Hurricane, R P Drake, H F Robey, C C Kuranz, B A Remington, M J Bono, M J Grosskopf, and R S Gillespie. Observation of a Kelvin-Helmholtz instability in a high-energy-density plasma on the Omega Laser. *Physical Review Letters*, 103:045005, 2009.

[11]C. C. Kuranz, R. P. Drake, E. C. Harding, M. J. Grosskopf, H. F. Robey, B. A. Remington, M. J. Edwards, A. R. Miles, T. S. Perry, T. Plewa, N. C. Hearn, J. P. Knauer, D. Arnett, and D. R. Leibrandt. 2D Rayleigh-Taylor instability: experiment and simulation. *Astrophysics Journal*, 696:749, 2009.

[12]R. Paul Drake. *High-Energy-Density Physics*. Springer, 2006.

[13]John T. Hunt and D. Ralph Speck. Present and future performance of the nova laser system. *Optical Engineering*, 28(4): 284461, 1989.

[14]T R Boehly, D L Brown, R S Craxton, R L Keck, J P Knauer, J H Kelly, T J Kessler, S A Kumpan, S J Loucks, S A Letzring, F J Marshall, R L McCrory, S F B Morse, W Seka, J M Soures, and C P Verdon. Initial performance results of the OMEGA laser system. *Optics Communications*, 133:495, 1997.

[15]Edward I. Moses and Craig R. Wuest. The National Ignition Facility: Status and plans for laser fusion and high-energy-density experimental studies. *Fusion Science and Technology*, 43(3):420–427, 2003.

[16]L Welser-Sherrill, J Fincke, F Doss, E Loomis, K Flippo, D Offermann, P Keiter, B Haines, and F Grinstein. Two laser-driven mix experiments to study reshock and shear. *High Energy Density Physics*, 9(3):496 – 499, 2013.

[17]F W Doss, E N Loomis, L Welser-Sherrill, J R Fincke, K A Flippo, and P A Keiter. Instability, mixing, and transition to turbulence in a laser-driven counterflowing shear experiment. *Physics of Plasmas*, 20:012707, 2013.

[18]F W Doss, J R Fincke, E N Loomis, L Welser-Sherrill, and K A Flippo. The high-energy-density counterpropagating shear experiment and turbulent self-heating. *Physics of Plasmas*, 20: 122704, 2013.

[19]E. Loomis, F. Doss, K. Flippo, and J. Fincke. Measurements of continuous mix evolution in a high energy density shear flow. *Physics of Plasmas*, 21:044508, 2014.

[20]Ye Zhou, Fernando F. Grinstein, Adam J. Wachtor, and Brian M. Haines. Estimating the effective Reynolds number in implicit large-eddy-simulation. *Phys. Rev. E*, 89:013303, 2014.

[21]B. M. Haines, F. F. Grinstein, L. W-Sherrill, J. R. Fincke, and F. W. Doss. Simulation ensemble for a laser-driven shear experiment. *Physics of Plasmas*, 20:092301, 2013.

[22]K. A. Flippo, F. W. Doss, B. Devolder, J. R. Fincke, E. N. Loomis, J. L. Kline, and L. Welser-Sherrill. Investigating turbulent mix in HEDLP experiments. *J. Phys.: Conf. Ser.*, 8th IFSA 2013:to be published, 2104.

[23]J. J. MacFarlane. VISRAD – a 3-D view factor code and design tool for high-energy density physics experiments. *Journal of Quantitative Spectroscopy & Radiative Transfer*, 81:287, 2003.

[24]E. L. Dewald, K. M. Campbell, R. E. Turner, J. P. Holder, O. L. Landen, S. H. Glenzer, R. L. Kauffman, L. J. Suter, M. Landon, M. Rhodes, and D. Lee. Dante soft x-ray power diagnostic for national ignition facility. *Review of Scientific Instruments*, 75 (10):3759, 2004.

[25]J. L. Kline, K. Widmann, A. Warrick, R. E. Olson, C. A. Thomas, A. S. Moore, L. J. Suter, O. Landen, D. Callahan, S. Azevedo, J. Liebman, S. H. Glenzer, A. Conder, S. N. Dixit, P. Torres, V. Tran, E. L. Dewald, J. Kamperschroer, L. J. Atherton, R. Beeler, L. Berzins, J. Celeste, C. Haynam, W. Hsing, D. Larson, B. J. MacGowan, D. Hinkel, D. Kalantar, R. Kauffman, J. Kilkenny, N. Meezan, M. D. Rosen, M. Schneider, E. A. Williams, S. Vernon, R. J. Wallace, B. Van Wonterghem, and B. K. Young. The first measurements of soft x-ray flux from ignition scale hohlraums at the national ignition facility using dante. *Review of Scientific Instruments*, 81(10):10E321, 2010.

[26]D Pellinen and Mathew Griffin. Response time measurements of the NIF DANTE XRD-31 x-ray diodes. Technical Report DOE/NV/25946–086, 2009.

[27]K A Flippo, J L Kline, F W Doss, E N Loomis, , M Emerich, B Devolder, T J Murphy K B Fournier, D H Kalantar, E Merritt, T S Perry, I Tregillis, L Welser-Sherrill, and J R Fincke. Development of a Big Area BackLighter (BABL) for high energy density experiments. *Review of Scientific Instruments*, 85:093501, 2014.

[28]Michael Gittings, Robert Weaver, Michael Clover, Thomas Betlach, Nelson Byrne, Robert Coker, Edward Dendy, Robert Hueckstaedt, Kim New, W Rob Oakes, Dale Ranta, and Ryan Stefan. The RAGE radiation-hydrodynamic code. *Computational Science and Discovery*, 1, 2008.

[29]John D. Lindl. *Inertial Confinement Fusion*. Springer, 1998.

[30]D. Ryutov, R. P. Drake, J. Kane, E. Liang, B. A. Remington, and W. M. Wood-Vasey. Similarity criteria for the laboratory simulation of supernova hydrodynamics. *Astrophysical Journal*, 518:821, 1999.

[31]D. D. Ryutov, B. A. Remington, H. F. Robey, and R. P. Drake. Magnetohydrodynamic scaling: From astrophysics to the laboratory. *Physics of Plasmas*, 8:1804, 2001.

[32]Ralph W. Metcalfe, Steven A. Orszag, Marc E. Brachet, Suresh Menon, and James J. Riley. Secondary instability of a temporally growing mixing layer. *Journal of Fluid Mechanics*, 184:207, 1987.